CERN-PH-TH-2015-056
TTP15-017

Higgs boson production in association with a jet at next-to-next-to-leading order

Radja Boughezal,[1,*] Fabrizio Caola,[2,†] Kirill Melnikov,[3,‡] Frank Petriello,[1,4,§] and Markus Schulze[2,¶]

[1] *High Energy Physics Division, Argonne National Laboratory, Argonne, IL 60439, USA*
[2] *CERN Theory Division, CH-1211, Geneva 23, Switzerland*
[3] *Institute for Theoretical Particle Physics, KIT, Karlsruhe, Germany*
[4] *Department of Physics & Astronomy, Northwestern University, Evanston, IL 60208, USA*

We present precise predictions for Higgs boson production in association with a jet. Our calculation is accurate to next-to-next-to-leading order (NNLO) QCD in the Higgs Effective Field Theory and constitutes the first complete NNLO computation for Higgs production with a final-state jet in hadronic collisions. We include all relevant phenomenological channels and present fully-differential results as well as total cross sections for the LHC. Our NNLO predictions reduce the unphysical scale dependence by more than a factor of two and enhance the total rate by about twenty percent compared to NLO QCD predictions. Our results demonstrate for the first time satisfactory convergence of the perturbative series.

Further exploration of the Higgs boson discovered by the ATLAS and CMS collaborations [1, 2] will be a primary goal of the continued experimental program of the LHC. In the well-measured decay modes, $h \to \gamma\gamma$, WW and ZZ, the determined couplings agree with the Standard Model (SM) values to $20-30$ percent [3, 4]. This agreement will be further probed during the upcoming LHC run. The predictions of the SM are expected to be tested to the five percent level in several production and decay modes [5], providing an exciting opportunity to discriminate between different mechanisms of electroweak symmetry breaking. In addition, new properties of the Higgs boson will be accessed through the measurement of its kinematic distributions. These measurements will test whether the tensor structures of the Higgs couplings are correctly predicted by the SM, whether additional operators mediate Higgs production and decay, and whether there are new particles that modify the loop-induced ggH and $\gamma\gamma H$ couplings.

Such studies [6] are currently limited by the available statistics. However, this situation will change during Run II of the LHC, and eventually the limiting factor in the search for deviations in Higgs boson properties from predictions will be our understanding of SM theory. This is apparent from a recent coupling combination performed by ATLAS [7]. The uncertainty on the theoretical predictions dominates the systematic error budget in all of the di-boson decay modes. One component of this error is the overall signal normalization, for which a precise calculation of inclusive Higgs production in the gluon-fusion channel is needed. The completion of the next-to-next-to-next-to-leading order ($\mathrm{N^3LO}$) calculation was recently announced [8]. The other major component of the theoretical error is the need for improved predictions of the differential spectra that enter every analysis. In some final states this need is obvious; for example, in the dileptonic decay of the WW channel a mass peak cannot be reconstructed, and accurate calculations of both signal and background distributions are needed in order to devise appropriate experimental search strategies. Even in modes where a resonance peak can be reconstructed, such as the $\gamma\gamma$ channel, the Higgs candidate events are categorized according to their transverse momentum ($p_\perp$) in order to improve the signal significance. Such a division relies upon accurate and precise theoretical predictions for the Higgs $p_\perp$ and rapidity distributions, that are used to reweight the parton-shower Monte Carlo simulations employed by the experimental collaborations.

In this Letter we take a major step toward improving SM predictions for several kinematic distributions employed in the analysis of Higgs boson properties, by providing a next-to-next-to-leading order (NNLO) calculation of Higgs boson production in association with a jet. Compared to previous computations [9, 10], we include all relevant channels and color structures. The phenomenological impact of this result spans all Higgs search channels. In the WW final state it refines the division of the signal prediction into exclusive zero-jet, one-jet and inclusive two-jet bins, and it can be used to improve the resummation of the jet-veto logarithms that accompany this division [11]. For all final states our calculation can be used to more accurately re-weight the Higgs $p_\perp$ distribution obtained from Monte Carlo. Finally, it will allow for the comparison of the measured differential distributions from LHC Run II with the most precise SM theory to more incisively probe the mechanism of electroweak symmetry breaking.

Our calculation also represents a technical milestone in the application of perturbative QCD to the modelling of hadronic collisions. The past few years have seen a renaissance in the development of subtraction techniques designed to turn our knowledge of the infrared structure of QCD at NNLO into actual phenomenological predictions for hadron-collider observables [9, 10, 12]. Our result demonstrates the power of these newly-developed methods in assisting the continued exploration of Nature at the LHC.

Our Letter is organized as follows. We first review the theoretical framework that we use to obtain the results reported in this paper. Since this has been described in

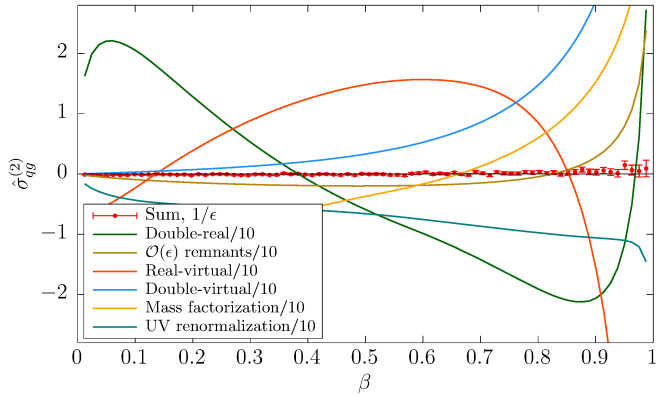

Figure 1: Cancellation of $1/\epsilon$ poles in the qg channel. Note that individual contributions have been rescaled by a factor of 0.1, while the sum of them is not rescaled.

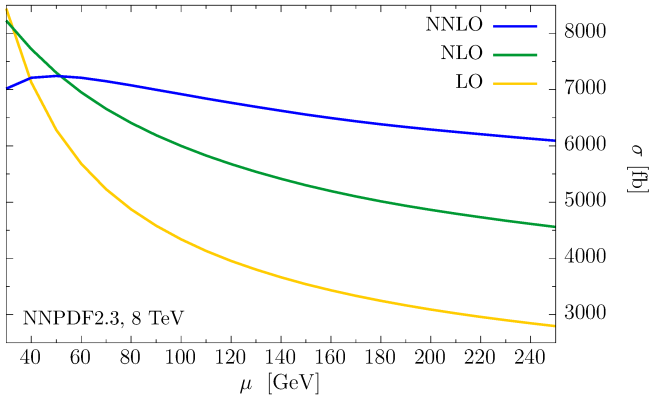

Figure 2: Dependence of the total LO, LO and NNLO cross-sections on the unphysical scale μ. See text for details.

detail in our previous work on Higgs plus jet production in pure gluodynamics [9], we only sketch here the salient features of the calculation. We then present the numerical results of the computation including NNLO results for cross sections of Higgs plus jet production at various collider energies and for various values of the transverse momentum cut on the jet. We also discuss the NNLO QCD corrections to the transverse momentum distribution of the Higgs boson. Finally, we present our conclusions.

We begin by reviewing the details of the computation. Our calculation is based on the effective theory obtained by integrating out the top quark. For values of the Higgs $p_\perp$ below 150 GeV, this approximation is known to work to 3% or better at NLO [13, 14]. Since the Higgs boson receives its transverse momentum by recoiling against jets, we expect that a similar accuracy of the large-m_t approximation can be expected for observables where jet transverse momenta do not exceed $\mathcal{O}(150)$ GeV as well.

The effective Lagrangian is given by

$$\mathcal{L} = -\frac{1}{4} G^{(a)}_{\mu\nu} G^{(a),\mu\nu} + \sum_i \bar{q}_i i \not{D} q_i - C_1 \frac{H}{v} G^{(a)}_{\mu\nu} G^{(a),\mu\nu}, \quad (1)$$

where $G^{(a)}_{\mu\nu}$ is the gluon field-strength tensor, H is the Higgs boson field and q_i denotes the light quark field of flavor i. The flavor index runs over the values $i = u, d, s, c, b$, which are all taken to be massless. The covariant derivative $\not{D}$ contains the quark-gluon coupling. The Higgs vacuum expectation value is denoted by v, and C_1 is the Wilson coefficient obtained by integrating out the top quark. The calculation presented here requires C_1 through $\mathcal{O}(\alpha_s^3)$, which can be obtained from Ref. [15]. Both the Wilson coefficient and the strong coupling constant require ultraviolet renormalization; the corresponding renormalization constants can be found e.g. in Ref. [16].

Partonic cross sections computed according to the above prescription are still not finite physical quantities. Two remaining issues must be addressed. First, contributions of final states with different number of partons must be combined in an appropriate way to produce infrared-safe observables. This requires a definition of final states with jets. We use the anti-k_T jet algorithm [17] to combine partons into jets. Second, initial-state collinear singularities must be absorbed into the parton distribution functions (PDFs) by means of standard $\overline{\rm MS}$ PDF renormalization. A detailed discussion of this procedure can be found in Ref. [18].

The finite cross sections for each of the partonic channels ij obtained in this way have an expansion in the $\overline{\rm MS}$ strong coupling constant $\alpha_s \equiv \alpha_s(\mu)$, defined in a theory with five active flavors,

$$\sigma_{ij} = \sigma^{(0)}_{ij} + \frac{\alpha_s}{2\pi}\sigma^{(1)}_{ij} + \left(\frac{\alpha_s}{2\pi}\right)^2 \sigma^{(2)}_{ij} + \mathcal{O}(\alpha_s^6). \quad (2)$$

Here, the omitted terms indicated by $\mathcal{O}(\alpha_s^6)$ include the α_s^3 factor that is contained in the leading order cross section $\sigma^{(0)}_{ij}$. Our computation will include the gg and qg partonic cross sections at NNLO, $\sigma^{(2)}_{gg}$ and $\sigma^{(2)}_{qg}$, where q denotes any light quark or anti-quark. At NLO, it can be checked using MCFM [19] that these channels contribute over 99% of the cross section for typical jet transverse momentum cuts, $p_\perp \sim 30$ GeV. We therefore include the partonic channels with two quarks or anti-quarks in the initial state only through NLO.

In addition to the ultraviolet and collinear renormalizations described above, we need the following ingredients to determine $\sigma^{(2)}_{gg}$ and $\sigma^{(2)}_{qg}$: the two-loop virtual corrections to the partonic channels $gg \to Hg$ and $qg \to Hq$; the one-loop virtual corrections to $gg \to Hgg$, $gg \to Hq\bar{q}$ and $qg \to Hqg$; the double real emission processes $gg \to Hggg$, $gg \to Hgq\bar{q}$, $qg \to Hqgg$ and $qg \to HqQ\bar{Q}$, where the $Q\bar{Q}$ pair in the last process can be of any flavor. The helicity amplitudes for all of these processes are available in the literature. The two-loop amplitudes were computed in Ref. [20]. The one-loop corrections to the four-parton processes are known [21] and

available as a Fortran code in the MCFM program [19]. For five-parton tree-level amplitudes, we use compact results obtained using BCFW recursions [22].

The difficulty in completing the NNLO calculation becomes apparent when one attempts to combine these contributions and cancel the infrared divergences that appear separately in each component. The problem is that final states with different multiplicities live in different phase-spaces; this feature makes it impossible to combine them directly. The issue becomes obvious if one looks at how $1/\epsilon$ singularities appear in different contributions. Indeed, the $1/\epsilon$ poles coming from loop amplitudes are explicit ones, but those coming from the real-emission corrections only appear upon integration over the unresolved region of phase space. However, since we want to keep the calculation fully differential, we want to avoid integrating over the phase-space for higher-multiplicity processes.

To reconcile these two requirements, which at first sight appear to be mutually exclusive, we use the sector-improved residue subtraction approach [23–26]. This is an outgrowth of the sector-decomposition method [27–29] used to compute the differential cross sections for Higgs boson and electroweak gauge bosons through NNLO. Sector decomposition uses the observation that the relevant singularities can be isolated using appropriate parameterizations of phase space and expansions in plus distributions. Sector-improved residue subtraction combines this with the idea that a pre-partitioning of the final-state phase space similar to the FKS subtraction used at NLO [30] allows to extend this technique to $2 \to 2$ and more complicated scattering processes. A detailed discussion of the phase-space parameterizations needed to handle all the contributing partonic processes was given in Ref. [9], to which we refer the reader for more details. Note, however, that Ref. [9] dealt with $gg \to H + ng$ partonic processes for which both the phase-space and the matrix elements are highly symmetric. For the quark-gluon channel this symmetry is lost and one has to consider a larger number of "sectors" compared to the case of pure gluodynamics.

Before discussing numerical results, we would like to point out two things in connection with the application of sector-improved residue subtraction method. First, we note that upon applying this method, one automatically generates subtraction terms that allow extraction of $1/\epsilon$ singularities and, at the same time, make integration of the finite remainders possible. The key point is that these subtraction terms are obtained from universal soft and collinear limits of scattering amplitudes that were computed long ago in Refs. [31–38]. The universality of these subtraction terms makes the method of improved-sector decomposition attractive and, in principle, applicable to processes of arbitrarily high multiplicity. Second, when sector-improved residue subtraction is applied to a physical process, it leads to a Laurent expansion of the various contributions to the cross section in the dimensional regularization parameter ϵ; the coefficients of this expansion are computed *numerically*. Since final physical cross sections are independent of the regularization parameter, the quality of $1/\epsilon^n$, $n = 4, 3, 2, 1$, cancellation is an important check of the correctness of the implementation of the method. To show the quality of the cancellation in our case, in Fig. 1 we present various contributions to the $1/\epsilon$ pole of the partonic cross section, together with the residual non-cancellation, in the qg channel. We show these quantities as functions of the distance from the partonic threshold, defined as $\beta = \sqrt{1 - s_{th}/\hat{s}}$, $\sqrt{s_{th}} = \sqrt{m_H^2 + p_{\perp,cut}^2} + p_{\perp,cut}$. We see that the cancellation is very good, at the level of one per mill or better. Although in Fig. 1 we display the result for the total cross section, we have also checked that the cancellation holds at a similar level for kinematic distributions.

In addition, we have checked that our results for the Higgs plus 2-jet cross section at NLO agree with MCFM [39], for both the fiducial cross section and for several kinematic distributions. We have two separate numerical implementations of the sector-improved residue subtraction method that demonstrate good agreement. Furthermore, an independent calculation was also performed using the jettiness-subtraction technique [40], and good agreement for the fiducial cross sections was found.

We now turn to the discussion of numerical results. We first compute the LO, NLO and NNLO cross sections for Higgs plus jet production $pp \to H + j$ at the 8 TeV and 13 TeV LHC. We use $m_H = 125$ GeV and $m_t = 172.5$ GeV. To define the cross section, we use the anti-$k_\perp$ algorithm with $\Delta R = 0.5$ and a cut on the jet transverse momentum $p_\perp > 30$ GeV. We employ parton distribution functions and the strong coupling constant as provided by the NNPDF21LO [41], NNPDF23NLO and NNPDF23NNLO [42] PDF sets to compute respectively LO, NLO and NNLO cross sections. We set the renormalization and factorization scales to the mass of the Higgs boson and we estimate the uncertainty associated with higher orders in perturbation theory by changing the scale by a factor of two. For the 8 TeV LHC, we find $\sigma_{pp\to H+j} = 3.9^{+1.7}_{-1.1}$ pb, $5.6^{+1.3}_{-1.1}$ pb, $6.7^{+0.5}_{-0.6}$ pb at leading, next-to-leading and next-to-next-to-leading order, respectively. Results for $\mu = m_H/2$ and $\mu = 2m_H$ are shown as super- and sub-scripts, respectively. For $\mu = m_H$, the NLO (NNLO) cross section exceeds the leading order one by 44% (72%), indicating reasonable convergence of perturbative expansion. The convergence is better for lower scales: for example, for $\mu = m_H/2$ the NLO (NNLO) cross section exceeds the leading order one by 23% (29%). As expected, the scale uncertainty is significantly reduced at NNLO. This is also illustrated in Fig. 2, where we plot the total cross section at LO, NLO

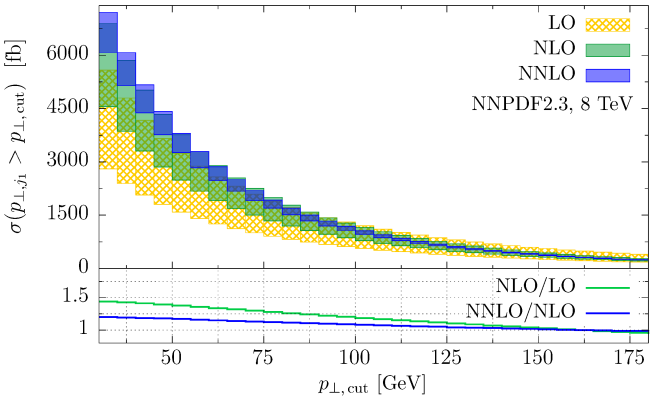

Figure 3: Higgs plus jet production cross-sections in dependence of the cut on the jet transverse momentum. The minimal cut we consider is $p_\perp > 30$ GeV. See text for details.

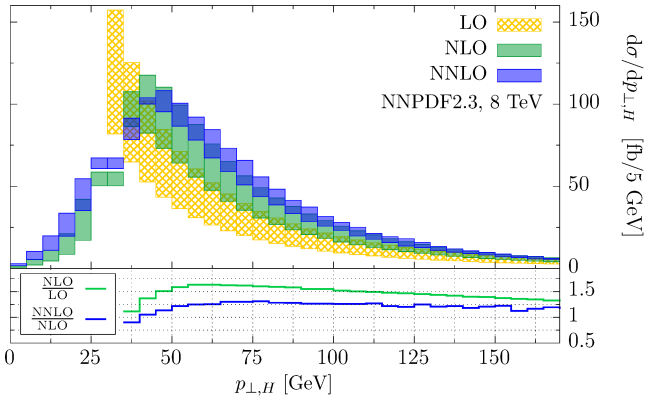

Figure 4: Higgs boson transverse momentum distribution in $pp \to H+j$ at 8 TeV LHC. The jet is defined with the anti-$k_\perp$ algorithm with $\Delta R = 0.5$ and the cut on the jet transverse momentum of 30 GeV. Further details are explained in the text.

and NNLO as a function of the unphysical scale μ over the range $\mu \in [p_{\perp,cut} : 2m_H]$. We estimate the residual uncertainty due to PDF to be at the $\mathcal{O}(5\%)$ level. The situation is similar for the 13 TeV LHC. More precisely, we find $\sigma_{pp\to H+j} = 10.2^{+4.0}_{-2.6}$ pb, $14.7^{+3.0}_{-2.5}$ pb, $17.5^{+1.1}_{-1.4}$ pb at leading, next-to-leading and next-to-next-to-leading order, corresponding to a NLO (NNLO) increase with respect to LO of 44% (72%) for $\mu = m_H$ and of 25% (31%) for $\mu = m_H/2$.

It is interesting to understand to what extent perturbative QCD corrections depend on the kinematics of the process and/or on the details of the jet algorithm. One way to study this is to explore how the NNLO QCD corrections change as the lower cut on the jet transverse momentum is varied. We show corresponding results for the 8 TeV LHC in Fig. 3 where the cumulative distribution for $\sigma(H+j, p_{\perp,j} \geq p_{\perp,\mathrm{cut}})$ is displayed. The inset in Fig. 3 shows ratios of NNLO(NLO) to NLO(LO) $H+j$ cross-sections, respectively, computed for $\mu_F = \mu_R = m_H$ as a function of the jet $p_\perp$-cut. It follows from Fig. 3 that QCD radiative corrections depend on the kinematics. Indeed, the NNLO to NLO cross-sections ratio changes from 1.25 at $p_\perp = 30$ GeV to ~ 1 at $p_\perp \sim 150$ GeV.

In Fig. 4 we show the Higgs boson transverse momentum distribution in the reaction $pp \to H + j$, for three consecutive orders of perturbation theory. We require that there is a jet in the final state with a transverse momentum higher than $p_{\perp,j} > 30$ GeV. Note that the two bins closest to the boundary $p_{\perp,H} = 30$ GeV have been combined to avoid the well-known Sudakov-shoulder effect [43]. Away from that region, the NNLO QCD radiative corrections increase the NLO cross-section by about 20%, slowly decreasing as $p_{\perp,H}$ increases.

In conclusion, we have presented a calculation of the NNLO QCD corrections to the production of the Higgs boson in association with a jet at the LHC. This is the first complete computation of NNLO QCD corrections to a Higgs production process with a jet in the final state. It shows that techniques for performing NNLO QCD computations, that were in the development phase for several years, can indeed be used to provide precise predictions for complex process at hadron colliders. The total cross section for H+jet production receives moderate NNLO QCD corrections. For jets defined with the anti-$k_\perp$ algorithm with $p_{\perp,j} > 30$ GeV, we find NNLO QCD corrections of the order of 20% for $\mu = m_H$. These moderate corrections are the result of the smaller corrections for the qg channel w.r.t the gg one, and a suppression of the gg channel due to $q\bar{q}$ final states not considered in previous analyses [9, 10]. Beyond the total cross section, our computation will have important implications for many processes that are used to study properties of the Higgs boson, including W^+W^- and $\gamma\gamma$ final states, primarily through improved modelling of the Higgs transverse momentum and rapidity distributions. In particular, since the complete N^{3}LO computation of the Higgs boson production cross section is available, a consistent computation of the $H+0$ jets, $H+1$ jet, $H+2$ jet and $H+3$ jet exclusive processes becomes possible for the first time. Furthermore, since the Higgs boson is a spin-zero particle, our computation can be easily extended to include Higgs boson decays, to enable theoretical predictions for fiducial cross sections and kinematic distributions for the particles that are observed in detectors. Once this is done, our calculation will provide a powerful tool that will help to understand detailed properties of the Higgs boson at the LHC.

We thank T. Becher, J. Campbell, T. Gehrmann and M. Jaquier for helpful communications. We are grateful to S. Badger for making his results for tree-level amplitudes available to us. F. C. would like to thank the Institute for Theoretical Particle Physics of KIT and the Physics and Astronomy Department of Northwestern University for hospitality at various stages of this project.

R. B. is supported by the DOE under the contract DE-AC02-06CH11357. F. P. is supported by the DOE grants DE-FG02-91ER40684 and DE-AC02-06CH11357. This research used resources of the National Energy Research Scientific Computing Center, a DOE Office of Science User Facility supported by the Office of Science of the U.S. Department of Energy under Contract No. DE-AC02-05CH11231.

* Electronic address:rboughezal@anl.gov
† Electronic address:fabrizio.caola@cern.ch
‡ Electronic address:kirill.melnikov@kit.edu
§ Electronic address:f-petriello@northwestern.edu
¶ Electronic address:markus.schulze@cern.ch

[1] G. Aad *et al.* [ATLAS Collaboration], Phys. Lett. B 716 (2012) 1.
[2] S. Chatrchyan *et al.* [CMS Collaboration], Phys. Lett. B 716 (2012) 30.
[3] ATLAS Collaboration, ATLAS-CONF-2013-034.
[4] CMS Collaboration, CMS-PAS-HIG-13-005.
[5] S. Dawson, A. Gritsan, H. Logan, J. Qian, C. Tully, R. Van Kooten, A. Ajaib and A. Anastassov *et al.*, arXiv:1310.8361 [hep-ex].
[6] See, for example, the following study of differential distributions in the $\gamma\gamma$ and $4l$ channels: ATLAS Collaboration, arXiv:1504.05833 [hep-ex].
[7] ATLAS Collaboration, ATLAS-CONF-2014-009.
[8] C. Anastasiou, C. Duhr, F. Dulat, F. Herzog and B. Mistlberger, arXiv:1503.06056 [hep-ph].
[9] R. Boughezal, F. Caola, K. Melnikov, F. Petriello and M. Schulze, JHEP **1306**, 072 (2013).
[10] X. Chen, T. Gehrmann, E. W. N. Glover and M. Jaquier, Phys. Lett. B **740**, 147 (2015).
[11] A. Banfi, G. P. Salam and G. Zanderighi, JHEP **1206**, 159 (2012). A. Banfi, P. F. Monni, G. P. Salam and G. Zanderighi, Phys. Rev. Lett. **109**, 202001 (2012). X. Liu and F. Petriello, Phys. Rev. D **87**, 014018 (2013). X. Liu and F. Petriello, Phys. Rev. D **87**, no. 9, 094027 (2013). T. Becher, M. Neubert and L. Rothen, JHEP **1310**, 125 (2013). I. W. Stewart, F. J. Tackmann, J. R. Walsh and S. Zuberi, Phys. Rev. D **89**, 054001 (2014). R. Boughezal, X. Liu, F. Petriello, F. J. Tackmann and J. R. Walsh, Phys. Rev. D **89**, 074044 (2014).
[12] A. Gehrmann-De Ridder, T. Gehrmann, E. W. N. Glover and J. Pires, Phys. Rev. Lett. **110**, no. 16, 162003 (2013). M. Czakon, P. Fiedler and A. Mitov, Phys. Rev. Lett. **110**, no. 25, 252004 (2013). J. Currie, A. Gehrmann-De Ridder, E. W. N. Glover and J. Pires, JHEP **1401**, 110 (2014). M. Brucherseifer, F. Caola and K. Melnikov, Phys. Lett. B **736**, 58 (2014). M. Czakon, P. Fiedler and A. Mitov, arXiv:1411.3007 [hep-ph]. R. Boughezal, C. Focke, X. Liu and F. Petriello, arXiv:1504.02131 [hep-ph].
[13] R. V. Harlander, T. Neumann, K. J. Ozeren and M. Wiesemann, JHEP **1208**, 139 (2012).
[14] S. Dawson, I. M. Lewis and M. Zeng, Phys. Rev. D **90**, no. 9, 093007 (2014)
[15] K. G. Chetyrkin, B. A. Kniehl and M. Steinhauser, Nucl. Phys. B **510**, 61 (1998).
[16] C. Anastasiou and K. Melnikov, Nucl. Phys. B **646**, 220 (2002).
[17] M. Cacciari, G. P. Salam and G. Soyez, JHEP **0804**, 063 (2008).
[18] S. Buehler and A. Lazopoulos, JHEP **1310**, 096 (2013).
[19] J. M. Campbell and R. K. Ellis, Nucl. Phys. Proc. Suppl. **205-206**, 10 (2010).
[20] T. Gehrmann, M. Jaquier, E. W. N. Glover and A. Koukoutsakis, JHEP **1202**, 056 (2012).
[21] C. F. Berger, V. Del Duca and L. J. Dixon, Phys. Rev. D **74**, 094021 (2006) [Erratum-ibid. D **76**, 099901 (2007)]. S. D. Badger and E. W. N. Glover, Nucl. Phys. Proc. Suppl. **160**, 71 (2006). S. D. Badger, E. W. N. Glover and K. Risager, JHEP **0707**, 066 (2007). E. W. N. Glover, P. Mastrolia and C. Williams, JHEP **0808**, 017 (2008). S.D. Badger and E.W.N. Glover, P. Mastrolia and C. Williams, JHEP **1001**, 036 (2010). L. J. Dixon and Y. Sofianatos, JHEP **0908**, 058 (2009). S. Badger, J. M. Campbell, R. K. Ellis and C. Williams, JHEP **0912**, 035 (2009).
[22] S. D. Badger, unpublished.
[23] M. Czakon, Phys. Lett. B **693**, 259 (2010).
[24] M. Czakon, Nucl. Phys. B **849**, 250 (2011).
[25] R. Boughezal, K. Melnikov and F. Petriello, Phys. Rev. D **85**, 034025 (2012).
[26] M. Czakon and D. Heymes, Nucl. Phys. B **890**, 152 (2014).
[27] T. Binoth and G. Heinrich, Nucl. Phys. B **680**, 375 (2004).
[28] C. Anastasiou, K. Melnikov and F. Petriello, Phys. Rev. D **69**, 076010 (2004).
[29] T. Binoth and G. Heinrich, Nucl. Phys. B **693**, 134 (2004).
[30] S. Frixione, Z. Kunszt and A. Signer, Nucl. Phys. B **467**, 399 (1996).
[31] S. Catani, D. de Florian, and M. Grazzini, Nucl. Phys. B **596** (2001) 299.
[32] F. A. Berends and W.T. Giele, Nucl. Phys. B **313**, 595 (1989).
[33] J.M. Campbell and E.W.N. Glover, Nucl. Phys. B **527**, 264 (1998).
[34] S. Catani and M. Grazzini, Phys. Lett. B **446**, 143 (1999).
[35] Z. Bern, *et al.* Phys. Rev. D **60**, 116001 (1999).
[36] S. Catani and M. Grazzini, Nucl. Phys. B **570**, 287 (2000).
[37] S. Catani and M. Grazzini, Nucl. Phys. B **591**, 435 (2000).
[38] D. A. Kosower, P. Uwer, Nucl. Phys. B **563**, 477-505 (1999).
[39] J. M. Campbell, R. K. Ellis and G. Zanderighi, JHEP **0610**, 028 (2006) [hep-ph/0608194].
[40] R. Boughezal, C. Focke, X. Liu and F. Petriello, in preparation.
[41] R. D. Ball, V. Bertone, F. Cerutti, L. Del Debbio, S. Forte, A. Guffanti, J. I. Latorre and J. Rojo *et al.*, Nucl. Phys. B **849**, 296 (2011).
[42] R. D. Ball, V. Bertone, S. Carrazza, C. S. Deans, L. Del Debbio, S. Forte, A. Guffanti and N. P. Hartland *et al.*, Nucl. Phys. B **867**, 244 (2013).
[43] S. Catani and B. R. Webber, JHEP **9710**, 005 (1997).